Refractive index discontinuities in fiber optic connectors

N. LAMBRACHE[*], J. PEREIRA[a], A. TOROBIN[b]
Alef Photonics, Ottawa, Canada
[a]*Alef Photonics, Ottawa, Canada*
[b]*Alef Photonics, Ottawa, Canada*

Connector loss variability has an important impact on planning and developing fiber optics networks. Interdisciplinary design considering optical and contact mechanics phenomena at the interface between connected waveguides with physical contact is a key element in providing sound recommendations for technology. The authors focus on studying the influence of refractive index discontinuities occurring on fiber optic connectors with physical contact and suggest design and manufacturing approaches for controlling it.

1. Losses in fiber optic connectors

Power losses in fiber optic connectors with physical contact are caused by a large number of factors such as: *End Gaps*, *Core* and *Numerical Aperture Mismatch*, *Axial Run-out,* End Angle, *End-face Roughness*, *Dust*, etc. [1].

End gaps between fiber optic connector end-faces are particularly important because they cause both Optical Return Loss (RL) and Optical Insertion Loss (IL). Minimizing RL on high-speed DWDM systems is particularly important in stabilizing the central wavelength of the laser sources. RL is usually expressed as the ratio between the input power P_i and the reflected power P_r and is expressed in decibels (dB) [2]:

$$RL = 10\log_{10}\frac{P_i}{P_r} \qquad (1)$$

The optical return loss RL can be reduced significantly by ultra polishing end-faces in contact as in UPC connectors and even by angling them as schematically represented in Figure 1, as in APC connectors. Most authors agree with values of 35 dB to 55 dB for UPC connectors and 55 dB to 70 dB for APC connectors [2].

Optical Insertion Loss or IL is the direct result of inserting a device in the transmission line and is defined as the ratio between the signal power before attaching a device, P_t, and the signal power received after inserting the device, P_r, and is expressed in decibels [2]:

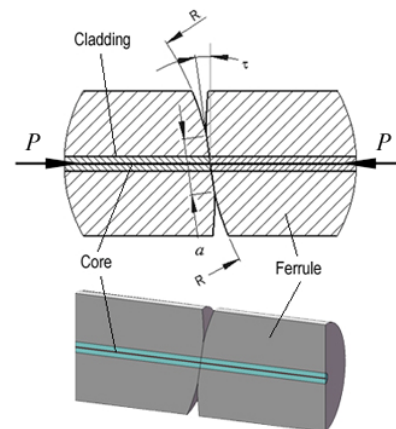$$IL = 10\log_{10}\frac{P_t}{P_r} \qquad (2)$$

Fig. 1. Angled end-faces in physical contact.

The authors investigate the effects of refractive index discontinuities on connectivity performance of SC PC connectors for single mode Corning SMF 28 step-index fiber working at the wavelength λ =1550 nm. The 3D model of typical SC PC connectors is represented in Fig. 2. Under the load of a helical compression spring, the system ferrule – fiber is pressed against another similar system of the same type. The core and cladding of the fiber are made of fused silica glass (SiO_2) of high chemical purity. Its optical specifications related to the paper are as follows:

- Mode-Field Diameter MDF at λ =1550 nm: 10.4±0.8 μm
- Core Diameter: 8.2 μm
- Cladding Diameter: 125.0±0.7 μm

- Effective Group Index of Refraction at nominal MFD: 1.4682 nm
- Refractive Index Difference: 0.36%
- Numerical Aperture: 0.14

The ferrule which guides the fiber is made of zirconia or zirconium oxide (ZrO_2). The material offers excellent polishing efficiency and finishes. However, the material is not suitable for outdoor employment because of the flattening effect, probably a result of surface shift from tetragonal to monoclinic crystalline forms under combined effects of load, temperature and humidity gradients [3].

A comprehensive account of all connector losses should consider ferrule and fiber geometric tolerances involved in a total run-out. However, this paper limits itself to the investigation of the effects of loaded end-face geometry on optical performance of the connector.
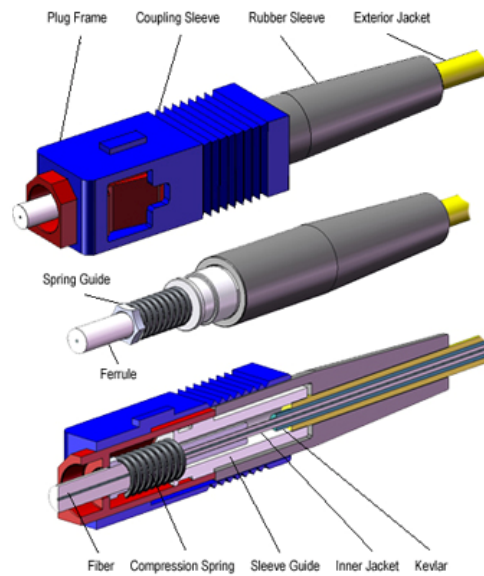

Fig. 2. 3D model of generic SC PC connector.

2. Modelling air-gap discontinuities

Air-gaps resulting from under-cut polishing of fiber connector end-faces are a major source of signal loss. A better understanding of light wave propagation in those arbitrary waveguide geometries is thus needed [4].

Numerical solutions to the paraxial approximation of the Helmholtz equation for monochromatic waves are based on finite difference beam propagation method as described in [5]. By restricting the wave propagation to narrow angles and neglecting polarization effects, the scalar field assumption is valid and the wave equation can be written in the known Helmholtz form:

$$\frac{\partial^2 \phi}{\partial x^2} + \frac{\partial^2 \phi}{\partial y^2} + \frac{\partial^2 \phi}{\partial z^2} + k^2(x, y, z)\phi = 0 \quad (3)$$

For most guided-wave problems, the fastest variation of the field ϕ is the phase variation due to propagation along the guiding axis. Assuming the guiding axis is z, this fast variation can be factored out by introducing a slowly varying field $u(x, y, z) = \phi(x, y, z)/e^{i\vec{k}z}$. $\vec{k}$ is the reference wavenumber and represents the average variation of the field ϕ. It is common practice to express the wavenumber in terms of a reference refractive index $\vec{n}$ as in $\vec{k} = k_0\vec{n}$. Under these assumptions one can write the three dimensional Beam Propagation Method (BPM) equation:

$$\frac{\partial u}{\partial z} = \frac{i}{2\vec{k}}\left(\frac{\partial^2 u}{\partial x^2} + \frac{\partial^2 u}{\partial y^2} + \left(k^2 - \vec{k}^2\right)u\right) \quad (4)$$

For a given input field $u(x, y, z = 0)$, the BPM equation (04) describes the evolution of the field in the space $z > 0$. Furthermore, the 3D equation (04) can be simplified for 2D by omitting all dependencies on y.

Simulation settings:
- Free Space Wavelength: λ =1550 nm
- Background Refractive Index: 1.4682
- Refractive Index Difference: 0.005
- Waveguide Width:
- Profile: Step Index
- 3D Structure: Fiber
- Cover Refractive Index: 1
- Crank-Nicholson Implicit Scheme
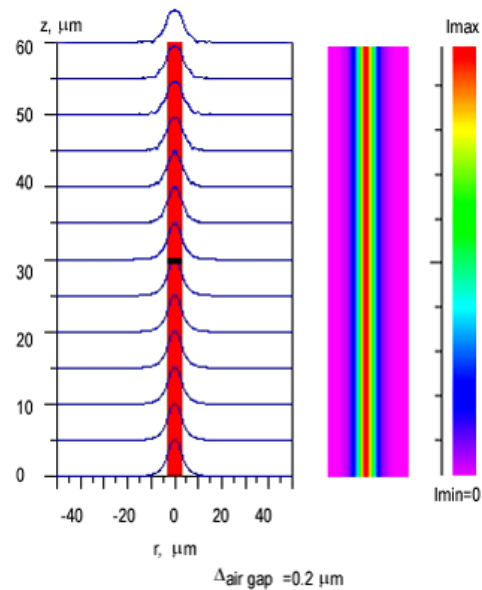- Full Transparent Boundary Condition
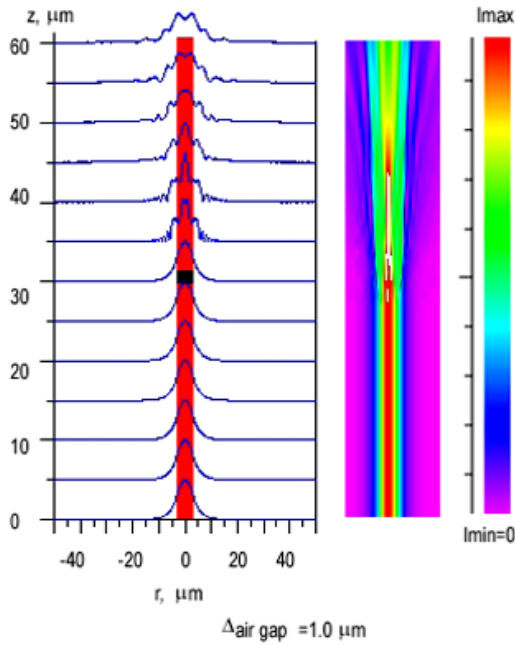- Padé Order: (4,4)

Fig. 3. BMP with air-gap Δ=0.2μm.

Fig. 4. BMP with air-gap $\Delta=1\mu m$.

Fig. 3 shows a practically non-altered beam mode profile after propagation through an air-gap $\Delta=0.2\mu m$. A seriously altered beam mode profile after propagation through an air-gap $\Delta=1\mu m$ is shown in Fig. 4. The simulation is performed in BeamProp and shows non-acceptable degradation levels of the beam mode profile for cylindrical air-gaps $\Delta>0.5\text{-}0.6\mu m$.

3. Contact mechanics in connectors

In fiber optic connectors with physical contact, localized stresses develop as the two curved surfaces in contact deform slightly under the normal load. The deformations are dependant of the geometry of surfaces in touch, their modulus of elasticity, and the applied normal load [5]. The following assumptions are considered for Hertzian contacts:

- Strains are within the elastic limits
- Surfaces are frictionless, continuous and non-conforming
- Contact area is much smaller than the effective radius of the surfaces involved

The study of contact becomes complex if these assumptions are violated and the contact is considered non-Hertzian.
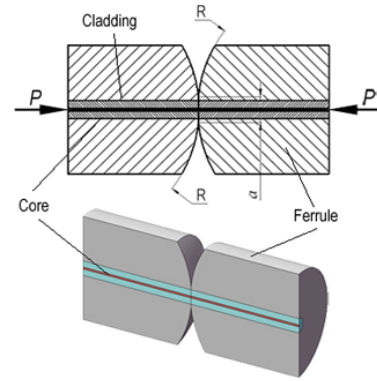

Fig. 5. Schematic representation of ferruled fibers in contact.

For a Hertzian contact between two spherical surfaces of radii R_1 and R_2, the area of contact has a circular shape of radius a and the distribution of pressure as a function from the center of the circle is given by [5]:

$$p(r) = p_0 \left(1 - \frac{r^2}{a^2}\right)^{\frac{1}{2}} \qquad (5),$$

p_0 is the maximum contact pressure and is given by:

$$p_0 = \frac{3P}{2\pi a^2} = \frac{1}{\pi}\left(\frac{6PE^{*2}}{R_e^2}\right)^{\frac{1}{3}} \qquad (6)$$

In fiber optic connectors the materials in contact are identical and have the same Poisson ratio ν. In equation (06), E^* represents the effective elastic modulus, given by:

$$E^* = \frac{E}{2\left(1-\nu^2\right)} \qquad (7)$$

R_e represents the effective radius, given by:

$$R_e = \frac{R_1 R_2}{R_1 + R_2} \qquad (8)$$

The radius of contact area is related to the applied load P by the equation:

$$a = \left(\frac{3PR_e}{4E^*}\right)^{\frac{1}{3}} \qquad (9)$$

Finally, the depth of indentation is given by the equation:

$$d = \frac{a^2}{R_e} = \left(\frac{9P^2}{16R_e E^{*2}} \right)^{\frac{1}{3}} \qquad (10)$$
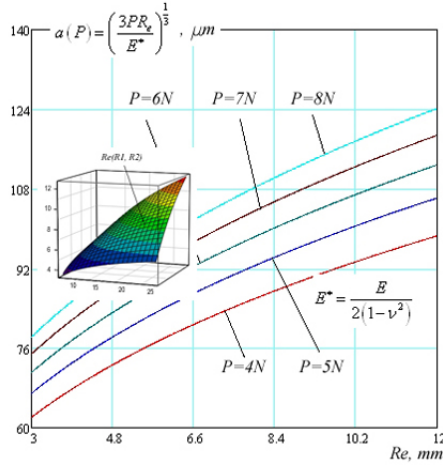

Fig. 6. Radius of contact area as function of R_e and load.

The graphs in Fig. 6 are traced for fused silica glass with Poisson ratio $\nu = 0.17$ and Young's effective modulus $E^* = 73000 N/mm^2$. For spherically shaped end-faces with radii between 10mm and 25mm, the equivalent radius varies between 3mm and 12mm. For small loads and small effective radii the radius of area of contact has values close to the radius of the cladding, and may create marginal air-gaps with the potential of influencing the beam propagation. As a safety precaution, it is a good approach to avoid such situations by increasing the load or by selecting mating surfaces with radii away from the 10-12mm range.

Equation (9) is valid for smooth surfaces in contact. Rough surfaces diminish the predicted size of contact area. [5]. Elevated roughness induces increased interface air-gaps and affects the optical performance of the connector.

Two surfaces in close proximity are the subject of attractive van der Waals forces and tend to adhere. The Hertz model does not consider adhesion. However, experimental approaches are suggesting significant deviations from the elastic model:

- Under small loads the contact area is larger than the Hertz model predictions
- Strong adhesion effects are present if the mating surfaces are dust-free and dry
- The contact area is non-zero even when the load is removed.

On a positive note, adhesion increases the contact area between the mating optical surfaces. However, repeated mating of dust-free and dry end-faces will alter their geometry and will reduce the lifespan of the connectors.
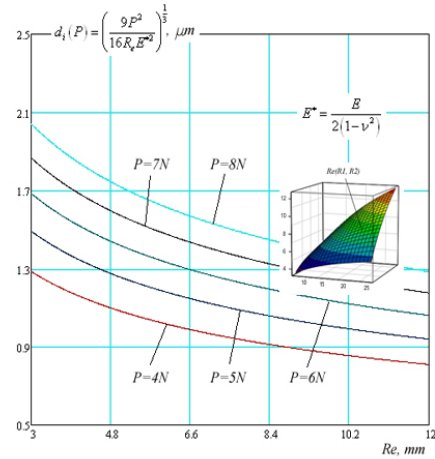

Fig. 7. Indentation as function of R_e and load.

The graphs in Fig. 7 are also traced for fused silica glass with Poisson ratio $\nu = 0.17$ and Young's effective modulus $E^* = 73000 N/mm^2$. The indentation has values in the range of microns; it alters the isotropy of materials in contact and induces birefringence in fused silica. Further research on this effect is required.

4. Technology requirements

Developing precision fiber optic connectors requires multidisciplinary design and sets up specific targets for manufacturing and metrology. The required specifications for connector end-faces are:

- Radii of curvature in the range 10mm – 25mm
- Spherical height $h = \pm 50 \mu m$
- Linear offset $l_o = \leq 50 \mu m$
- Roughness $R_q \leq 10 nm$ on both fiber and ferrule
- Loads in the range 5N-6N

These specifications place a great emphasis on the polishing and cleaning processes. Continual evaluation of the end-faces geometry during the polishing is essential.

The geometry for the end-faces can be controlled by employing a planetary movement, classical in optical technology. The parameters of the planetary movement required for generating the shape of the end-faces are to be optimized in accordance with Preston's theory:

$$h_{M_{(\rho,\theta)}} = C_T \int_T pv d\tau \qquad (11)$$

$h_{M_{(\rho,\theta)}}$ represents the linear quantity of material removed from the end-face at an arbitrary point $M_{(\rho,\theta)}$, C_T is a

constant of material, p is the pressure at $M_{(\rho,\theta)}$, v is the linear speed in $M_{(\rho,\theta)}$, τ is the time from the start of the process and T is the total polishing time.

The spherical shape of the end-face is a result of the interaction between the ferrule, the fiber and the rubber pad. The initial geometry of the ferrule, the nature of the materials involved, and the polishing procedures are all important.

Polishing experiments with a variety of materials like aluminium oxide, chrome oxide, cerium oxide, etc., proved to offer less satisfactory results compared to diamond. Diamond lapping films provide a dependable finish to surfaces of elevated hardness like zirconium oxide.

Wet polishing with 0.1μm diamond films and type I deionised water provides the optimal settings for the desired low roughness, as illustrated in Fig. 8. The microstructure of the surfaces is clearly visible at a magnification of 400X.

Geometry parameters characterizing polished connectors like radius of curvature, offset of polish, undercut or protrusion should be evaluated on non-contact and fully automatic interferometric microscopes. The system provides 3D topographic information regarding the geometry of the surface inspected. Real time access to the topology of the end-face gives the user full control of the polishing processes.
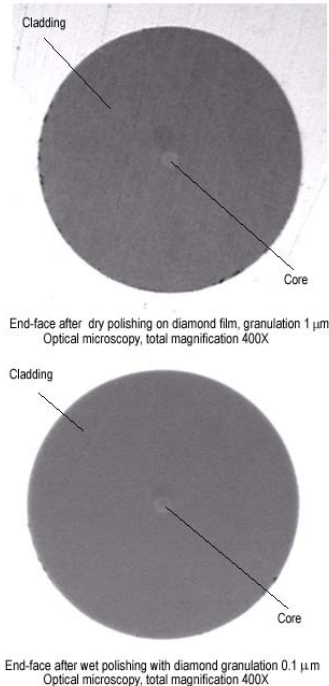

Fig. 8. End-face microscopy, magnification 400X.

Interferometric topography of polished end-face connector performed on such system is illustrated in Fig. 9. The user has real time access to valuable information regarding radii of curvature, spherical height, linear and angular offset, and ferrule and fiber roughness.
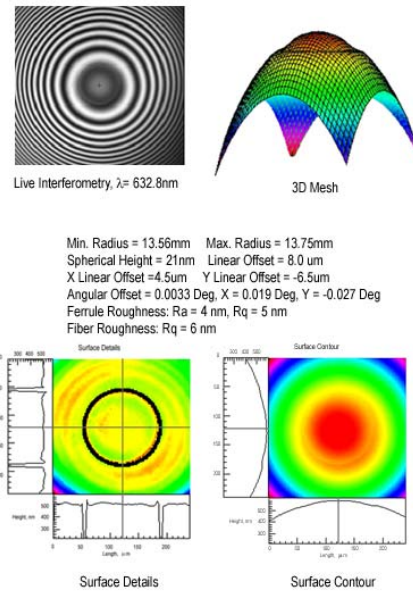

Live Interferometry, λ= 632.8nm   3D Mesh

Min. Radius = 13.56mm   Max. Radius = 13.75mm
Spherical Height = 21nm   Linear Offset = 8.0 um
X Linear Offset =4.5um   Y Linear Offset = -6.5um
Angular Offset = 0.0033 Deg, X = 0.019 Deg, Y = -0.027 Deg
Ferrule Roughness: Ra = 4 nm, Rq = 5 nm
Fiber Roughness: Rq = 6 nm

Surface Details   Surface Contour

Fig. 9. Interferometric inspection of polished end-face.

5. Concluding remarks

The authors emphasize the benefits of interdisciplinary efforts in developing optical waveguide connectors with physical contact and focus on the influences of refractive index discontinuities on transmission losses. Numerical modelling of such discontinuities using the finite difference beam propagation method allows accurate evaluations of the wave propagation through the air-gaps. Contact mechanics facilitates the understanding of loaded interface phenomena and suggests optimized end-face geometries. Finally, the authors comment on specific polishing challenges, and suggest consistent solutions.

References

[1] J. Crisp, Introduction to Fiber Optics, 3rd Edition, Newnes, Oxford, UK (2005).
[2] D. Goff, Fiber Optic Reference Guide, 3rd Edition, Elsevier Science, Woburn, Massachusetts, USA (2002).
[3] J. Shackelford, Materials Science and Engineering Handbook, 3rd Edition, CRC Press, New York, USA(2001).
[4] B. Saleh, M. Teich, Fundamentals of Photonics, John Wiley & Sons, New York, USA (1991).
[5] K. L. Johnson, Contact Mechanics, Cambridge University Press, Cambridge, UK (1985).

[*]Corresponding author: Nicholas.Lambrache@alefphotonics.com